Particle simulation of plasma heat-flux dissipation by evaporated wall materials

K. Ibano[1], T. Takizuka[1], D. Nishijima[2], J.H. Yu[2], M.J. Baldwin[2], R.P. Doerner[2], H.T. Lee[1], and Y. Ueda[1]

[1]Graduate School of Engineering, Osaka University, Suita, Osaka, 556-0871, Japan

[2]Center for Energy Research, University of California in San Diego, La Jolla, CA.92093-0417, USA

E-mail contact of main author: kibano@eei.eng.osaka-u.ac.jp

Abstract. Behaviors of wall-originated impurities are studied by a particle simulation in order to understand erosion processes during the fusion reactor operation. The particle simulations solves the particle motions in the vicinity of wall in a consistent manner with the sheath and pre-sheath potential drops. First, the effect of the potential drops for the prompt re-deposition is studied for Tungsten (W) walls. Then, the particle simulation is applied for the vapor shield experiments taken at the PISCES-B linear plasma. The experimentally indicated T_e drop by Beryllium (Be) vapor is simulated. Comparison between Be and W vapor showed that the ionization mean free path determines the radiation volume thus the lighter Be is effective for the plasma cooling. In order to confirm these effects in the fusion devices, the heat flux by an ELMy plasma at a divertor is simulated by using high energetic electron and ions.

1. Introduction

Large erosions of the wall materials via melting, sputtering, and vaporization are concerned to be caused by the intense pulsed heat loads during ELMs and disruption in the fusion devices. These erosion shortens the life time of components and thus increases maintenance frequency. Thus, predictions of erosion rates should be precisely taken. During these intense plasma heat loads, a self-shielding behavior was observed by vapor layer formation on the wall surface. [1–3] Then, experimental and computational simulation efforts were taken to study this phenomenon. A fluid element model simulation of the vapor shielding effect for a graphite wall was achieved and reported in [4]. However, these fluid code cannot include the sheath and non-Maxwellian effects in general. It is expected that these effects are not negligible for the behaviors of high-Z materials such as tungsten (W). Thus, demands for a particle-in-cell (PIC) simulation of the vapor shielding are being increased. We have been developed a PIC code for the plasma-vapor interaction. In this paper, details of simulation models are described first (Section 2). Then, we report (1) prompt re-deposition behavior of W particle(Section 3), (2) difference of plasma cooling abilities between beryllium (Be) and W vapors as observed in experiments at PISCES-B and corresponding PIC simulations (Section 4) and (3) heat flux simulation in the ELMy plasma (Section 5).

2. Particle-in-Cell code model description

We adopt a one-dimensional (1D) open plasma system in a magnetic field for the PIC simulation of the vapor shielding as shown in Fig. 1. A code consists of one dimensional for space and three dimensional for velocity (1d3v). Up to five different species of super-particles are treated in this study, e.g., background electron and ions, wall impurity species, and ELM

electron and ions. Basic calculation schemes are similar with the ES1 code [5], but the non-uniform weighting of super-particles is the specialty.

Each super-particle individually labeled j with a mass m_j, a charge number Z_j, and a density weight w_j, is moved in accordance with the equation of motion,

$$m_\mathrm{j}\frac{\mathrm{d}\boldsymbol{v}_\mathrm{j}}{\mathrm{d}t} = Z_\mathrm{j}e(\boldsymbol{E} + \boldsymbol{v}_\mathrm{j} \times \boldsymbol{B}) \tag{1}$$

$$\frac{\mathrm{d}x_\mathrm{j}}{\mathrm{d}t} = v_{x,\mathrm{j}} \tag{2}$$

where $\boldsymbol{v}_\mathrm{j}$ is the velocity and x_j is the position. The uniform magnetic field $\boldsymbol{B}$ = (B_x, 0, B_z) is given. The electric field $\boldsymbol{E} = -\nabla\phi$ (ϕ is the electrostatic potential) is self-consistently solved by the 1D Poisson equation

$$\frac{\mathrm{d}^2\phi}{\mathrm{d}x^2} = -\frac{1}{\varepsilon_0}\sum_\mathrm{j} Z_\mathrm{j}e\, w_\mathrm{j}\,(x_\mathrm{j}) \tag{3}$$

where the sum in RHS represents the charge density, and its value on every mesh point is calculated with the usual PIC area-weighting scheme.

Based on the cross section data obtained from the OPEN-ADAS library [6], ionization and recombination reactions are simulated by the Monte-Carlo method. In the atomic-collision model, total collisionality of particle is calculated then the occurrence of the ionization/recombination reactions is determined based on a random number. In order to minimize the statistical errors, weighted particles are used for the low-density impurity particles. Then special treatment is applied for these atomic-process scheme. When using impurity particles with a small weighting, an ionization reaction produces an electron super particle with a same small weighting which is significantly smaller than the background plasma electron particles. Continuous generation of these tiny electron particles leads increasing calculation time. Thus, instead of generating new super particles, a corresponding weighting is attached to a nearby electron super-particle. For the recombination scheme, a corresponding weighting is removed from a nearby electron super-particle. Thus, eventually all super-particles have different weighting as calculation continues. In order to treat this atomic-process model, the code treats weighting (w_j), mass (m_j) and electric charge number (Z_j) as particle variables and individually recorded.

In the calculation, the central region of the system is treated as a region for the heating and the particle source (see Fig. 1). Heating is applied by a Langevin model [7] given as

$$\frac{\Delta\boldsymbol{v}_j}{\Delta t} = -\nu\boldsymbol{v}_\mathrm{j} + \boldsymbol{A} \tag{4}$$

$$\langle A\rangle = 0, \qquad \langle A^2\rangle = \frac{2T_{L0}}{m_j}\frac{\nu}{\Delta t} \tag{5}$$

where Δt is time step, T_{L0} is temperature, ν is a relaxation frequency and $\boldsymbol{A}$ is a random acceleration given by uniform random number (< > denotes the mean value). A particle source is set in the same region. When an electron and an ion reach a boundary, a pair of electron and ion comes back to the region together. If only electron reaches the boundary, it stays to be out of system and waits until an ion coming. This re-fueling scheme prevents shortages of particles in the system. It is noted that neutral impurities with Z_j = 0 are treated with the same equations (1)-(3) excluding the Langevin heating Eq. (4).

At the beginning of calculations, background electrons and ions are uniformly distributed in space with a Maxwellian velocity distribution in a designated temperature. As calculation continues with the heating and particle source regions, the system becomes steady-state. Once a steady-state condition is achieved, several testing, i.e., W prompt re-deposition testing, Be and W vapor shield testing, and ELM plasma testing are introduced.

Typical simulated plasma profiles are summarized in Fig. 2. All of these parameters are averaged values for 1000 time iterations. The heating and particle source is located in the position between 0.04 and 0.06 m. From the left and right boundary wall to the heating region, the Debye sheath and pre-sheath region can be clearly observed. The Mach number at the sheath entrance $M \geq 1$ at the sheath entrance, thus the Bohm criterion is satisfied. The Mach number can exceed unity in a sheath region because mean parallel random energies are used for the sound speed (C_s) definition.

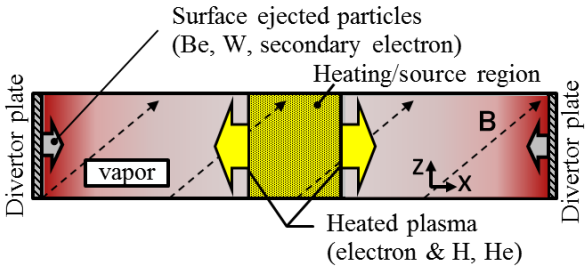

Fig. 1 Schematic view of the simulation system

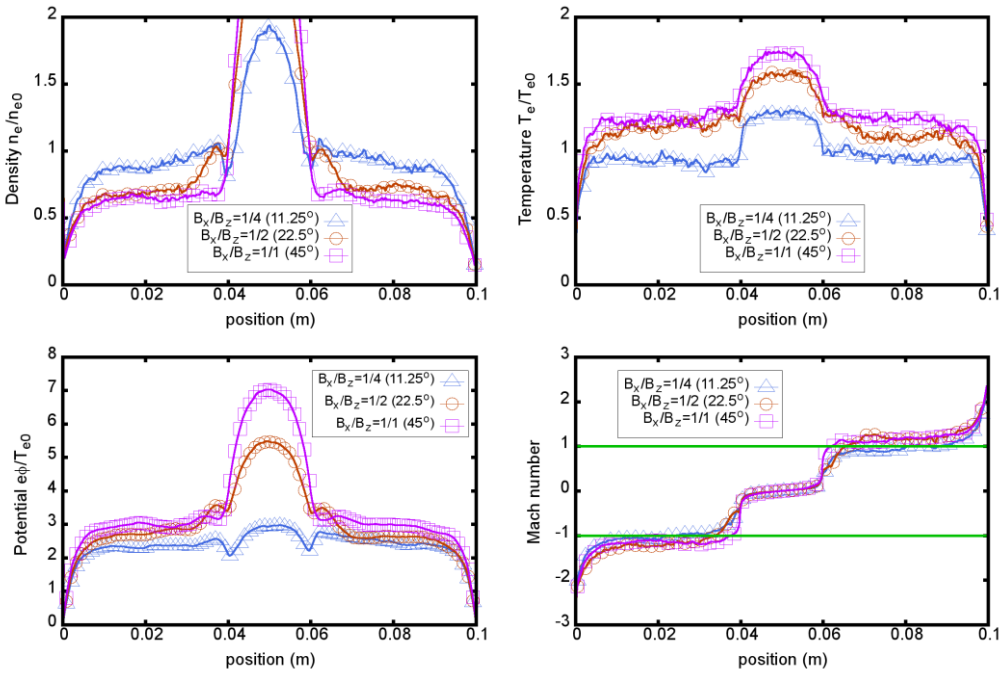

Fig. 2 Density, temperature, potential, and Mach number profiles of the background plasma at a steady-state condition. Different angles of the magnetic flux to the surface, 11.25°, 22.5° and 45° are shown with triangle, circle and square, respectively.[8]

3. Prompt re-deposition simulation

3.1. Prompt re-deposition test model

After the steady-state hydrogen plasma condition is achieved, W test particles are released from the wall boundaries. Then their projected distance as well as landing locations are recorded. A W particle is recorded as the prompt re-deposition if the distance between the particle and the surface at the far most projected point is smaller than the gyro radius at the point. Rest of re-deposited particles is recorded as the non-prompt re-deposition. A W particle is recorded as the non-redeposited if the particle reaches the heating region and removed from the calculation system. It is expected that the re-deposition of W particles strongly depend on the sheath potential. Thus, we introduce virtually "non-$q\boldsymbol{E}$ force" W test particles, which do not feel the $q\boldsymbol{E}$ force but feel the $q\boldsymbol{v}\times\boldsymbol{B}$ force. Using these virtual particles, re-deposition probability as a function of impurity ejection angles are examined. Simulations are taken for different angles of magnetic field line to the surface from 14° to 45° which corresponds experimental conditions at a linear device [9].

3.2. Comparisons between re-depositions of normal and non-$q\boldsymbol{E}$ force particle

In the prompt re-deposition simulations, an artificial factor for the ionization and recombination cross sections $\eta\langle\sigma v\rangle$ is assumed. This factor can change the ionization mean free path without changing the plasma condition. A parametric scan for the ionization m.f.p. is crucial since this factor strongly influence the re-deposition rate. Especially the ratio between gyration radius ρ_{gyro} and ionization m.f.p. λ_{ion} is the most important. Changing the artificial factor, $10^{-4}<\eta<10^{1}$, the parameter, $\rho_{\mathrm{gyro}}/\lambda_{\mathrm{ion}}$ is scanned. As shown in Fig. 3., total W re-deposition rates (filled marks) drops as the ratio $\rho_{\mathrm{gyro}}/\lambda_{\mathrm{ion}}$ decreases. For the higher ratio, the total re-deposition rate becomes close to unity while the non-prompt re-deposition rate (open marks) decreases. In contrast, in the case of the "non-$q\boldsymbol{E}$ force" particles (Fig.4), the total reposition rates does not reach unity even for the ratio $\rho_{\mathrm{gyro}}/\lambda_{\mathrm{ion}}>100$. Thus, it can be concluded here that the sheath potential has a dominant effect on the W prompt re-deposition.

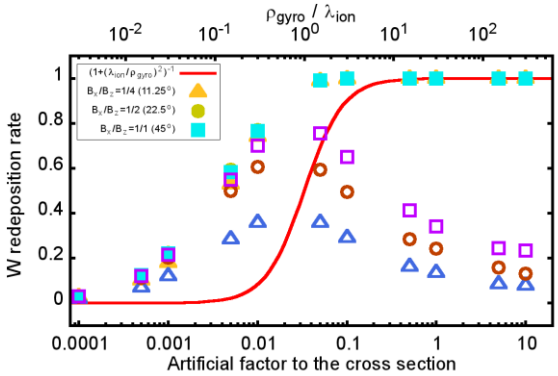

Fig. 3 W re-deposition rate as a function of the η value. Normal W particles with the Coulomb force are used in the simulation. Filled marks indicate total re-deposition and open marks indicate non-prompt re-deposition rate. [8]

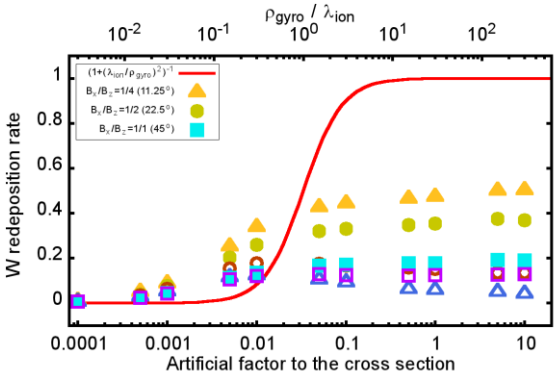

Fig. 4 W re-deposition rate as a function of the η value. The "non-q$\boldsymbol{E}$ forced" W particles are used in the simulation. Filled marks indicate total re-deposition and open marks indicate non-prompt re-deposition rate. [8]

4. PIC simulation for the vapor shielding experiments at PISCES-B

PISCES-B has a plasma source with a LaB_6 cathode generated arc plasma. Axial magnetic fields of 0.015 T were applied in order to confine the plasma. The typical plasma parameters at the target were 6.5 eV electron temperature, 10^{19} m^{-3} electron density and 10^{23} $m^{-2}s^{-1}$ ion flux. Nd:YAG laser (NEC M801C, 1064 nm wavelength) was aligned on the target surface. The laser shots can apply up 50 J energy to the target for the 10-20ms duration. Vapor ejection from the surface was confirmed for both W and Be targets by the high-speed camera images and the spectroscopy. When W vapor was generated, the decay length of neutral line emission from the surface decreased compared with the decay length of sputtered W neutrals. In contrast, when Be vapor was generated, the decay length of neutral Be line emission increases during laser shots. However, this increasing decay length was not observed when smaller laser energy shots were applied to the Be target. Thus, it was assumed that the significant amounts of Be vapor decreases the plasma temperature and ionization m.f.p. of the vapor Be particles increase.

In order to explain this experimental observation, PISCES-B plasma is simulated by the PIC code. In the simulation, the left boundary is treated as the biased sample target with -100 volts. Using a similar heating and particle source region as explained in the previous section, the steady-state He plasma is simulated. Once the plasma reaches a steady-state condition, W or Be impurity is emitted from the left boundary. The energy of emitted impurities is kept at 0.1 eV for both cases. Results are compared in Fig. 5. Simulated profiles of electron temperature T_e, total radiation power P_{rad}, total impurity density n_I, and impurity neutral density n_{I0} at the time 12 μs after the impurity ejection are summarized in the figures. In case of the Be emission, it is observed that Be density n_{Be} spreads up to x ~ 1 cm and T_e drops clearly due to the Be line radiation. In contrast, the W density n_W is well localized within <<1 cm from the surface. A W atom is about 20 times heavier and ionization rate coefficient is 2 times larger than Be atom, thus its ionization m.f.p is about 10 times shorter. Then the most of emitted W particles are ionized in the vicinity of the wall and re-deposited to the wall by the pre-sheath potential as discussed in the previous section. The shorter projected distance of the W particles results shorter radiation volume. Thus, even with the same vapor ejection rates for Be and W, the different results in plasma heat-flux dissipation are obtained for two cases.

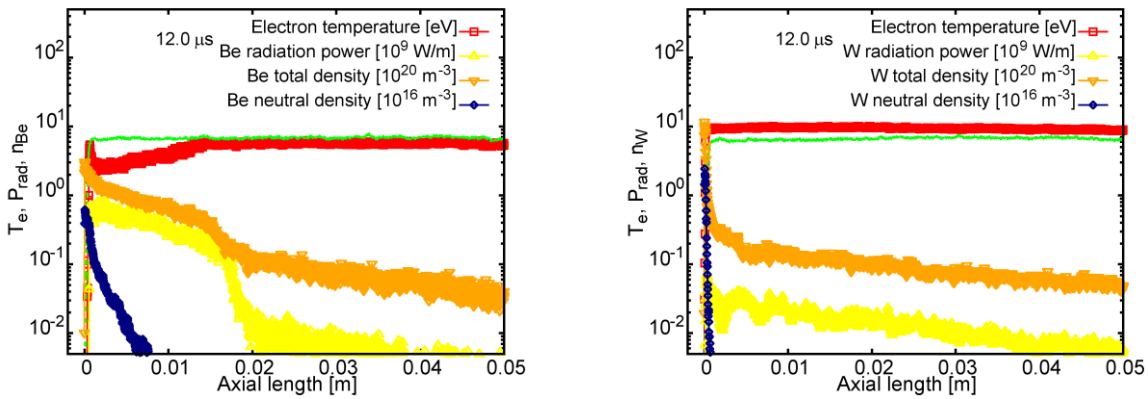

(a) (b)

Fig. 5 Simulated profiles of electron temperature (red), total impurity radiation power (yellow), total impurity density (orange), and impurity neutral density (navy) 12 μs after the impurity ejection of (a) 2×10^{23} Be/m^2s and (b) 2×10^{23} W/m^2s in the 10^{19} m^{-3} electron density plasma. Green line indicates T_e profile at the steady-state before the impurity ejection.

5. Vapor shielding simulation in an ELMy plasma condition

Energetic particle loads from the edge plasma at ELM will result a significant erosion of wall. In order to reveal their influences to the vapor shielding, a PIC simulation for an ELMy reactor plasma condition is carried out. In case of an unmitigated type-I ELM, 10^{24} $m^{-2}s^{-1}$ flux of particles with a few keV energy can reach the divertor wall. The high energy electrons from the edge plasma are transferred faster than the ions in the scrape-off-layer. Thus, the electrons arrives a few tens or hundreds μs earlier than the ions [10]. Fast electrons heat up the wall surface which causes melting and evaporation. Plus, these electrons grow the sheath potential. The higher sheath potential leads higher ion incident energy which leads larger sputtering amounts. In the PIC simulation, mono-energetic ELM electron/ion particles are introduced in addition to the background plasma and wall impurity particles. First, ELM electrons are injected into the source region of the PIC calculation domain after the background plasma becomes a steady-state condition. Then, ELM ions are injected into the source region after an artificial delay time from the ELM electrons injection. Heat flux by these particles and angle of incidence of ions are simulated in consistent with the potential profile.

PIC calculations for a 1 keV mono-energetic ELM flux into a n_e = 10^{19} m^{-3}, T_e = 50 eV steady-state plasma are taken. Time evolution of the heat flux on the divertor target is plotted in Fig. 6. First, ELM electrons are introduced from t = 125 μs, and 50 μs later (from t = 175 μs) ELM ions are supplied in the source region. During only ELM electrons are present (125 μs < t < 175 μs), the sheath potential increases and background ions get higher energy. As ELM ions reaches the target, the plasma potential returns to ~100 V.

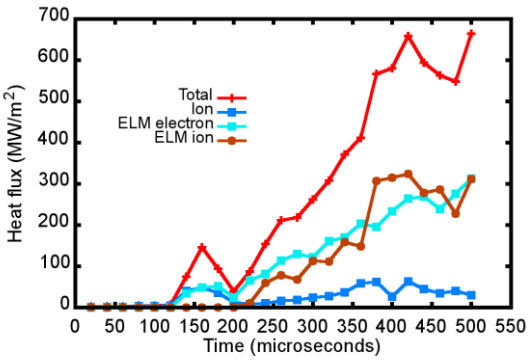

Fig. 6 Time evolution of the heat flux on the divertor tile. ELM starts at t = 125 μs with the introduction of 1keV fast electrons into a steady-state plasma n_e=10^{19} m^{-3}, T_e = 50 eV. ELM ions are supplied 50 μs later (t = 175 μs).

6. Summary and Conclusion

The 1d3v particle simulations are carried out. Applying the non-uniform weighting, the code follows particle dynamics with atomic processes related to the wall-originated impurities. At first, the re-deposition of W impurities is examined, and the role of the sheath and pre-sheath potential drop is clarified. Then, paying attention to the sheath effects, the difference in the

PISCES-B experimental results between Be- and W- vapor is examined. Once vapor particles are ionized, the sheath and pre-sheath potential drop pulls back these charged ions. Thus, a longer m.f.p. of the lighter Be vapor results a larger radiation volume for the plasma cooling, while little cooling by W vapour. Finally, the effect of the ELM on the vapour shielding in a fusion reactor is simulated by introducing transiently energetic electrons and ions. When large amount of Be is evaporated from the divertor plate by the fast arriving ELM electrons, significant radiation is expected to reduce the later arriving ELM heat flux.

Acknowledgement

This work is partly supported by Japan / U. S. Cooperation in Fusion Research and Development, JSPS KAKENHI Grant Number 25249132, and by the US DOE Grant: DE-FG02-07ER54912.

Reference

[1] Sakuma I, Kikuchi Y, Kitagawa Y, Asai Y, Onishi K, Fukumoto N and Nagata M 2015 Experimental investigation of vapor shielding effects induced by ELM-like pulsed plasma loads using the double plasma gun device *J. Nucl. Mater.* **463** 233–236

[2] van Eden G G, Morgan T W, Aussems D U B, van den Berg M A, Bystrov K and van de Sanden M C M 2016 Self-Regulated Plasma Heat Flux Mitigation Due to Liquid Sn Vapor Shielding *Phys. Rev. Lett.* **116** 135002

[3] Tereshin V I, Bandura A N, Byrka O V, Chebotarev V V, Garkusha I E, Landman I, Makhlaj V A, Neklyudov I M, Solyakov D G and Tsarenko A V 2007 Application of powerful quasi-steady-state plasma accelerators for simulation of ITER transient heat loads on divertor surfaces *Plasma Phys. Control. Fusion* **49** A231–239

[4] Genco F and Hassanein A 2014 Simulation of damage to tokamaks plasma facing components during intense abnormal power deposition *Fusion Eng. Des.* **89** 335–341

[5] Birdsall C K and Langdon A B 2005 *Plasma physics via computer simulation* (New York: Taylor & Francis)

[6] Summers H P and O'Mullane M G 2011 Atomic data and modelling for fusion: The ADAS Project *AIP Conference Proceedings* vol 1344pp 179–187

[7] Froese A, Takizuka T and Yagi M 2010 Effect of Source and Sink on Heat Transport in the SOL *Contrib. Plasma Phys.* **50** 273–278

[8] Ibano K, Togo S, Lang T L, Ogawa Y, Lee H T, Ueda Y and Takizuka T 2016 Simulations of Tungsten Re-deposition Using a Particle-In-Cell Code with Non-uniform Super Particle Sizes *Contrib. Plasma Phys.* **56** 705-710

[9] Kojima M, Ido Y, Ezumi N, Ohno N and Takamura S 1997 Erosion and Redeposition Processes of Molybdenum with Oblique Incidence of Magnetic Field *J. Plasma Fusion Res.* **73** 452–459

[10] Takizuka T and Hosokawa M 2006 Particle Simulation of the Transient Behavior of One-Dimensional SOL-Divertor Plasmas after an ELM Crash *Contrib. Plasma Phys.* **703** 698–703